

The dissipation of wind wave energy across a fringing reef at Ipan, Guam

A.-C. Péquignet · J. M. Becker ·
M. A. Merrifield · S. J. Boc

Received: 17 September 2010/Accepted: 2 January 2011/Published online: 21 January 2011
© Springer-Verlag 2011

Abstract Field observations over a fringing reef at Ipan, Guam, during trade wind and tropical storm conditions are used to assess the transformation of sea and swell energy from the fore reef to the shoreline. Parameterizations of wave breaking and bottom friction developed for sandy beaches are found to represent the observed decay in wave energy with an increased friction coefficient. These parameterizations are incorporated into the one-dimensional energy flux balance, which is integrated across the reef to assess the effects of varying tidal range, incident wave height and reef bathymetry on the sea and swell band wave height and wave setup near the shoreline. Wave energy on the reef is strongly depth-limited and controlled by the reef submergence level. Shoreline wave energy increases with incident wave height largely due to the increase in water level from breaking wave setup. Increased tidal levels result in increased shoreline energy, since wave setup is only weakly reduced. The wave height

at the shore is shown to be inversely proportional to the width of the reef flat due to dissipation.

Keywords Fringing reef · Hydrodynamics · Waves · Wave setup · Sea level · Friction · Wave breaking

Introduction

Wave transformation processes on various reef geometries have been the focus of field and laboratory studies (e.g., Tait 1972; Gerritsen 1981; Young 1989; Hardy and Young 1996; Kench 1998; Lowe et al. 2005; Gourlay and Colleter 2005; Kench and Brander 2006). Monismith (2007) and Hearn (2011) provide two excellent overviews of reef hydrodynamics. Wave breaking over shallow reef topography tends to account for the majority of energy dissipation in the sea and swell (SS) frequency band (0.06–0.3 Hz) (Young 1989; Hardy and Young 1996; Massel and Gourlay 2000). As the incident waves propagate into shallow water on the reef flat, frictional effects become increasingly important. On some barrier reefs, friction has been shown to be the dominant dissipative process (Lowe et al. 2005). As incident waves break at the reef face, radiation stress gradients force the setup of the sea surface shoreward of the break zone (Munk and Sargent 1948; Bowen et al. 1968; Gourlay 1996a, b; Vetter et al. 2010). The near-shore region of shallow reefs tends to be dominated by long waves at infragravity (IG) frequencies (e.g., Young 1989; Lugo-Fernandez et al. 1998b), similar to the swash zone of dissipative sandy beaches (Raubenheimer and Guza 1996; Ruggiero et al. 2004).

The transmission of SS energy toward shore is affected by water level over reefs, with increasing wave energy on

Communicated by Guest Editor Dr. Clifford Hearn

A.-C. Péquignet (✉) · M. A. Merrifield
Department of Oceanography, University of Hawaii at Manoa,
1000 Pope Road, Honolulu, HI 96822, USA
e-mail: chrispeq@hawaii.edu

M. A. Merrifield
e-mail: markm@soest.hawaii.edu

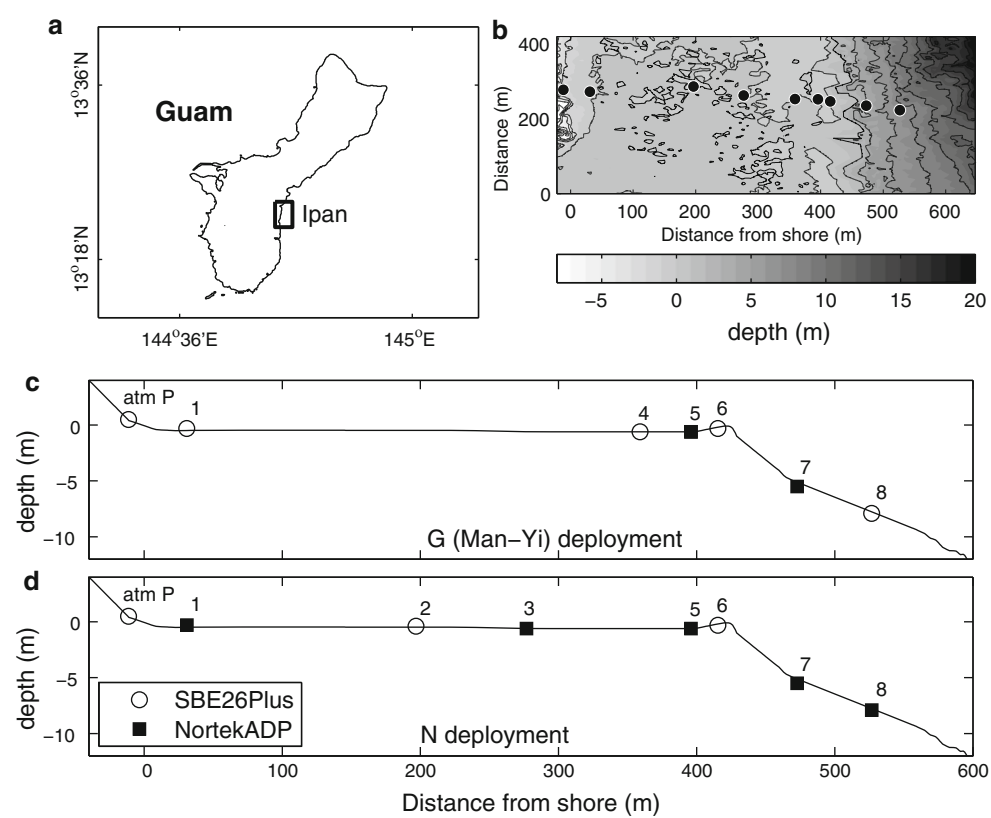
J. M. Becker
Department of Geology and Geophysics, University of Hawaii at Manoa, 1680 East West Rd, Honolulu, HI 96822, USA
e-mail: jbecker@soest.hawaii.edu

S. J. Boc
US Army Corps of Engineers, 4155 E.Clay Street,
Vicksburg, MS 39183, USA
e-mail: Stanley.J.Boc@usace.army.mil

reef flats observed for increasing tidal level (Young 1989; Hardy and Young 1996; Lugo-Fernandez et al. 1998a; Brander et al. 2004). During large wave events, wave setup may exceed the highest tidal range (Péquignet et al. 2009). Estimates of wave transformation and dissipation on reefs have been evaluated primarily using laboratory data (e.g., Gourlay 1996a, b; Gourlay and Colleter 2005; Massel and Gourlay 2000). Most observational studies to date have captured only moderate wave events and limited sea level ranges, hence, open questions remain regarding the reef flat SS energy budget during large wave events that generate significant setup and conditions that may allow significant SS energy to reach the shore.

The goal of this paper is to analyze field observations of waves across a shore-attached fringing reef to account for the amount of SS energy that reaches the shore as a function of incident wave conditions, water level over the reef, and position on the reef flat. We first detail the field experiments at Ipan and the data analysis methods. The observations then are used to analyze wave dissipation on the fore reef and reef flat. The dissipation estimates are incorporated in the one-dimensional integration of the SS energy flux balance across the reef to examine the effects of varying wave height and water level on reef flat wave heights. We conclude with an assessment of the effects of reef flat water level on shoreline wave energy.

Fig. 1 **a** Location of Ipan reef, Guam. **b** Bathymetry of Ipan reef from SHOALS data with locations of sensors. Cross-shore profile of Ipan reef with locations of sensors for deployments **c** *G* (June–July 2007) and **d** *N* (September–November 2009). Black squares indicate collocated pressure sensors and current-meters (*Nortek ADP*) and the white circles indicate single pressure sensors (*SBE26plus*). The sensor-labeled ‘atm P’ is a *SBE26plus* deployed above sea level to measure atmospheric pressure



Field experiment and methods

Site and sensors

Data used in this study were collected as part of the Pacific Island Land–Ocean Typhoon (PILOT) project that is aimed at assessing coastal inundation at reef-fringed islands during large wave events. The study site at Ipan (Fig. 1), on the south shore of Guam ($13^{\circ} 22'20''\text{N}$, $144^{\circ} 46'30''\text{E}$), is composed of a steep (4° slope) fore reef with irregular and rough topography of ~ 100 m wavelength and ~ 5 m amplitude spur-and-groove coral structures extending from approximately 15 m depth (Fig. 2a) to the shallow crest at the reef edge (Fig. 2b). The reef crest is porous and covered by macro and coralline algae (Fig. 2c). The shallow 450-m wide-reef flat is a carbonate pavement covered by macro algae (Fig. 2d) extending from the reef crest to a narrow sandy beach (Burbick 2005). The tides in Guam are mixed with a mean range of 0.5 m and spring tide range of 0.7 m. The reef flat is mostly exposed at low tide. The eastern side of Guam is subject to trade winds and occasional tropical storms and typhoons (Lobban and Scheffter 1994), which have been responsible for significant wave overwash (Jaffe and Richmond 1993).

Offshore wave conditions were obtained from a Datawell directional wave buoy operated by the Scripps

Fig. 2 Photos of the substrate for four locations across the reef: **a** on the fore reef near sensor 7 in 5 meters of water, **b** at the reef crest near sensor 6 (scale the width of the bottom of the photo spans about 3 m), **c** on the outer reef flat near sensor 4 (scale the current-meter shown is 60 cm long), and **d** on the reef flat near sensor 1 (scale the yellow ruler is 30 cm long)

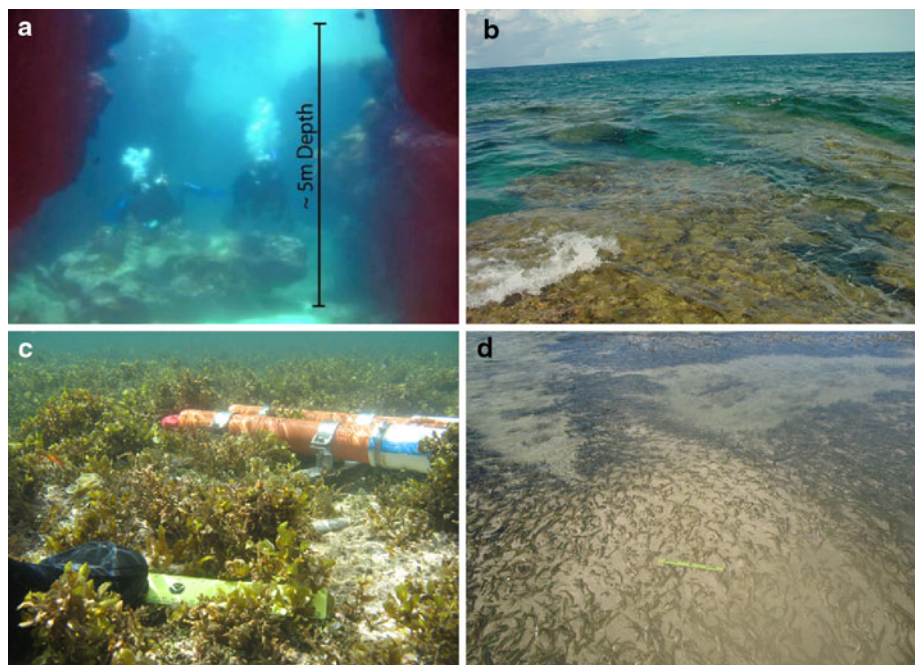


Table 1 Sensor location and sampling schemes for deployment *G* and *N*

Sensor number	Distance from shore (m)	Depth (m)	G burst	G velocity (m)	N burst	N velocity (m)
atm		0	P: 43,180 s/12 h		P: 43,180 s/12 h	
1	30	0.3	P: 43,180 s/12 h		PUV: 10,800 s/4 h	0.2:0.1
2	195	0.4			P: 43,180 s/12 h	
3	277	0.6			PUV: 10,800 s/4 h	0.2:0.1
4	359	0.6	P: 43,180 s/12 h			
5	399	0.6	PUV: 7,200 s/4 h	0.3:0.1	PUV: 10,800 s/4 h	0.2:0.1
6	416	0.3	P: 43,180 s/12 h		P: 43,180 s/12 h	
7	475	5.7	PUV: 7,200 s/4 h	1:1	PUV: 10,800 s/4 h	1:1
8	530	7.9	P: 43,180 s/12 h		PUV: 10,800 s/4 h	1:1

P a Seabird pressure sensor while *PUV* an Aquadopp velocity and pressure sensor. Length and frequency of bursts are indicated as length/frequency. Velocities measurements are specified by cell size: blanking distance

Institution of Oceanography Coastal Data Information Program (CDIP) located 2.4 km southeast of the reef array ($13^{\circ} 21'15''\text{N}$, $144^{\circ} 47'18''\text{E}$) in 200 m depth. CDIP provides time series of significant wave height, dominant wave direction, and wave period over 30-min intervals. An array of Seabird SBE 26Plus wave and water level recorders and Nortek Aquadopp Acoustic Doppler Profilers (ADP) was deployed across the reef, with two instruments on the fore reef and the remainder on the reef flat (Fig. 1). Deployments of 3–6 months of varying number of instruments and sampling schemes were carried out from August 2005 to April 2010. The 2 subsets of data used in this study were collected during June and July 2007 (deployment *G*) and from September to November 2009 (deployment *N*), which included a number of large wave events. The ADPs sampled at 1 Hz in bursts of 2 h every 3 h during *N* and every

4 h during *G*. All sensors sampled at 1 Hz, and sampling details and sensor locations are summarized in Table 1.

Pressure measurements were corrected for atmospheric pressure variations using a SBE 26Plus deployed on land (sensor atm *P*, Fig. 1). Using linear wave theory, sea surface elevations and surface velocities were estimated from bottom pressure and mid-column velocity. Changes in water temperature on the reef account for uncertainties of less than 0.2% in the estimation of sea surface elevation from the bottom pressure. At especially low tides, the reef flat sensors were exposed and these sections of data are not used in the analysis.

Spectral properties were estimated based on Fourier transforms of two-hour detrended and detided pressure data segments and band averaged using a Parzen spectral window, yielding approximately 22 degrees of freedom. Significant wave heights were estimated over 15-min intervals

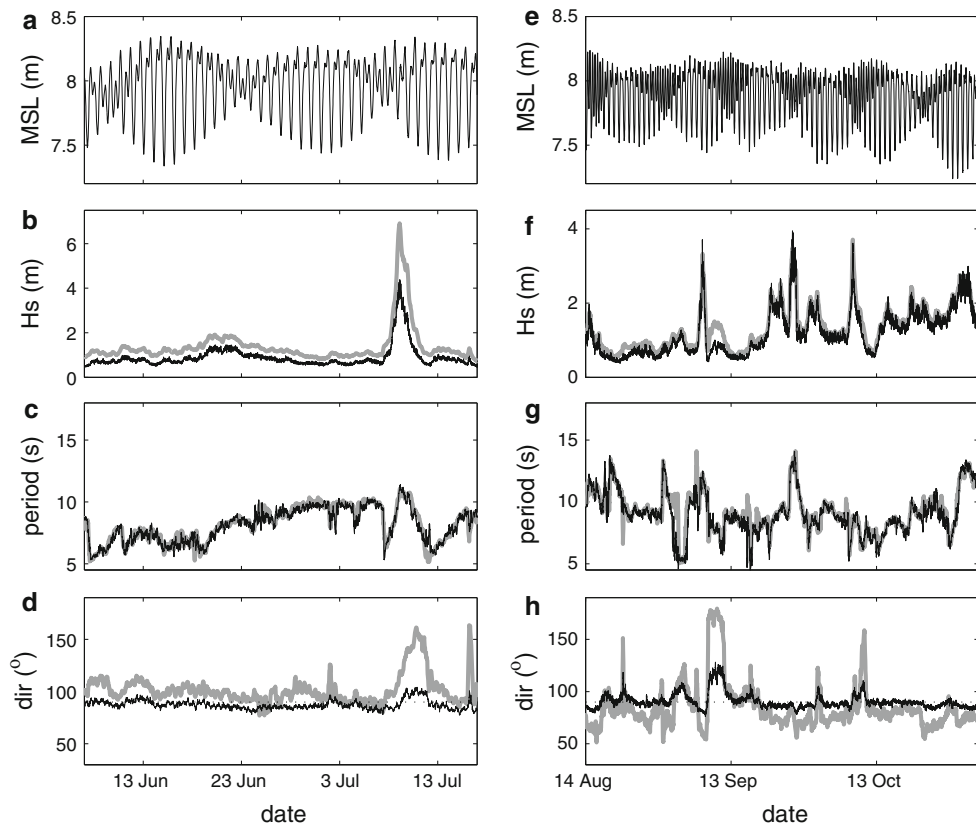


Fig. 3 Wave and water level conditions at the fore reef during deployment *G* (left panels June to July 2007) and deployment *N* (right panels August to November 2009), including **a** and **e** water level, **b** and **f** sea and swell (SS) band significant wave height, **c** and **g** the peak SS wave period, and **d** and **h** the incident SS wave angle

from the variance of sea surface elevation in the SS band ($0.06 \text{ Hz} < f < 0.3 \text{ Hz}$). Following Vetter et al. (2010), setup on the reef flat was estimated at reef flat sensors by taking the difference of the 15-min mean water level between the given sensor and sensor 8, with linear trends removed to account for sensor-related drifts in pressure that are unrelated to wave height. A linear trend was removed from all sensors for consistency, but the results are similar with or without the trend removal. An offset was specified so that setup is zero when incident wave heights at sensor 8 are zero.

During deployment *N*, typical trade wind conditions were observed with incident wind wave height in the 1–2 m range, and some energetic events reaching 4 m (Fig. 3e). Peak wave periods ranged from 5 to 15 s (Fig. 3f). The trade wind waves generally propagated from the ENE to ESE directions (Fig. 3c). Calm summer conditions during deployment *G* preceded tropical storm (later upgraded to typhoon) Man-Yi (July 9, 2007), which passed 200 nm south of Guam. Man-Yi resulted in offshore wave heights peaking at 7 m, peak period of 11 s, and wave arrivals from the SE (Fig. 3a, b, c). The large waves during this event led to high setup on

(relative to magnetic north) from the most offshore sensor (black line) and from the CDIP wave buoy (thick gray line). The variability of wave direction and period was smoothed by plotting the 6 h running mean for clarity of the figure

the reef (Péquignet et al. 2009) and inundation along some parts of the south shore of Guam. Observations of large wave events ($>2 \text{ m}$) were made at different phases of the tide (Fig. 3d, h). For both deployments, wave heights at the fore reef in 8 m depth tended to be weaker than wave heights at the wave buoy (Fig. 3a, e). This decrease in wave height depended on wave direction, and in particular, during Man-Yi when the waves came from the south, wave heights were 30% smaller at the fore reef than at the offshore buoy, presumably due to refraction effects.

Energy analysis

We evaluate the effects of wave dissipation in the context of changes in the cross-shore component of the energy flux, which is computed spectrally as

$$F_x(f) = 1/2 c_g(f) \rho g S_{\eta\eta}(f) \quad (1)$$

where ρ is the water density, g is the acceleration due to gravity, $c_g(f)$ is the group velocity, and $S_{\eta\eta}(f)$ is the auto-spectra of η . The angle of incidence at the most offshore current-meter location (Fig. 3d, h) was always within 15°

of shore normal due to wave refraction, and we assume that the energy flux is predominantly in the cross-shore direction. Comparison of computations of the vector energy flux at the ADPs with Eq. 1 supports the assumption that the flux is in the onshore direction.

With the assumption of normal incidence, and neglecting time-dependent changes in energy, the cross-shore component of the energy flux divergence in the SS band over a 1D bathymetry may be written as

$$\frac{dF_{\text{SS}}}{dx} = \langle \varepsilon_b \rangle + \langle \varepsilon_f \rangle + \langle N \rangle \quad (2)$$

where the SS energy flux F_{SS} is estimated by integrating Eq. 1 over the SS frequency band, and $\langle \varepsilon_b \rangle$ and $\langle \varepsilon_f \rangle$ are the average rates of dissipation per unit area due to wave breaking and bottom friction, respectively. $\langle N \rangle$ is the non-linear transfer of SS energy to other frequency bands, which has been observed previously on a reef during small wave conditions (Hardy and Young 1996).

Parameterizations of the energy loss due to wave breaking for sandy beaches have been applied to reef settings (Young 1989; Massel and Gourlay 2000). Here, we evaluate dissipation due to breaking following Thornton and Guza (1983). For a saturated wave field, the assumption that $H_b/h = O(1)$ near breaking (Baldock et al. 1998) reduces the average rate of dissipation to a quadratic function of breaking wave height H_b (Battjes and Janssen 1978)

$$\langle \varepsilon_b \rangle \approx B_r \rho g \bar{f} H_b^2 \quad (3)$$

where \bar{f} is the representative frequency of the random wave field and B_r is an empirical coefficient representing the fraction of foam on the wave face.

In addition, the parameterization of frictional dissipation also follows Thornton and Guza (1983)

$$\langle \varepsilon_f \rangle = \rho C_f \frac{1}{16\sqrt{\pi}} \left(\frac{2\pi\bar{f}}{\sinh kh} \right)^3 H_{\text{rms}}^3 \quad (4)$$

where h is the water depth, k is the wave number associated with \bar{f} and h , and $H_{\text{rms}} = 1/\sqrt{2}H_s$ is the root mean square wave height. The ratio of H_{rms}/H_s results from the wave height following a Rayleigh distribution. This assumption of Rayleigh distributed wave heights is valid on the fore reef and the reef flat. In the surf zone (sensors 5 and 6), the wave height distribution departs slightly from Rayleigh and this ratio may be underestimated (Massel 1996).

Results

Observations

A typical example of the power spectral density of sea surface elevation (Fig. 4) illustrates the change from short

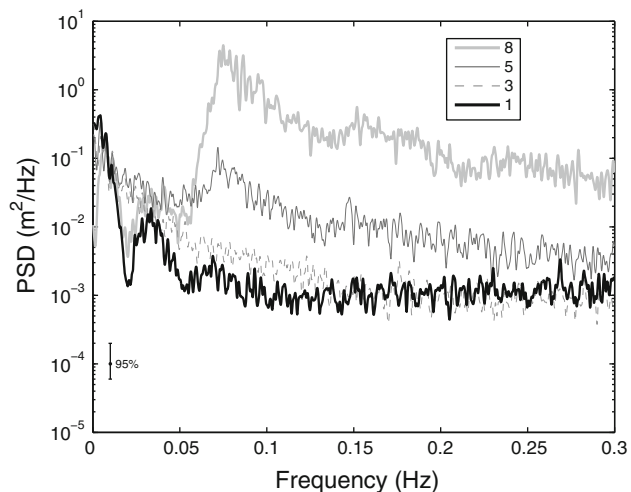


Fig. 4 Power spectral density of sea surface elevation at the fore reef (sensor 8), the reef crest (5), the outer reef flat (3), and the inner reef flat (1) during largest event of deployment N (October 2, 2009 21:00:00 UTM)

waves to long waves shoreward across the reef. On the fore reef (sensor 8), the wave field is dominated by SS oscillations with a peak frequency between 0.08 and 0.1 Hz. On the reef flat less than 10 m from the reef crest (sensor 6), the SS wave energy has decreased by nearly an order of magnitude, although the SS peak is still evident. At sensor 4, 57-m inshore of sensor 6, the SS energy is attenuated further, particularly at the incident spectral peak. Near the shoreline (sensor 1), the SS energy peak is absent. At IG frequencies (<0.06 Hz), energy levels at the fore reef (8) and outer reef (6 and 4) are comparable. At the shoreline (1), IG energy is lower than the outer reef and fore reef at frequencies >0.01 Hz, and higher at frequencies <0.01 Hz. In addition, the spectrum at sensor 1 exhibits a peak between 0.02 and 0.06 Hz, although the energy in this band still is significantly lower than farther offshore. The increasing relative importance of IG compared to SS oscillations with decreasing distance from the shore has been reported for other reefs (Hardy and Young 1996; Lugo-Fernandez et al. 1998a). The peak energy at 0.02–0.06 Hz may be associated with long incident SS waves or subharmonics of the incident peak over the reef. For this analysis, we will consider that energy as part of the IG band, which will be examined in a future study.

Mean water level near the shore (Fig. 5a) exhibits setup variations that scale with SS significant wave height on the fore reef (Fig. 5b). During large wave events, the setup exceeds the tidal range. Significant wave heights at the reef crest (sensor 5), mid-reef (3), and near the shore (1) show the nearly order of magnitude decrease in wave energy between the fore reef and reef crest, as well as the further dissipation of energy between the reef crest and the shore. The modulation of wave height with water depth is

Fig. 5 Time series during deployment N of **a** water depth on the reef at sensor 1, d_1 including both tidal and wave setup components, **b** incident significant wave height at sensor 8, H_{s8} and **c** wave heights on the reef flat at sensors 1, 3, and 5. Reef flat wave height plotted as a function of d_1 and H_{s8} for **d** sensor 1, **e** sensor 3, and **f** sensor 5

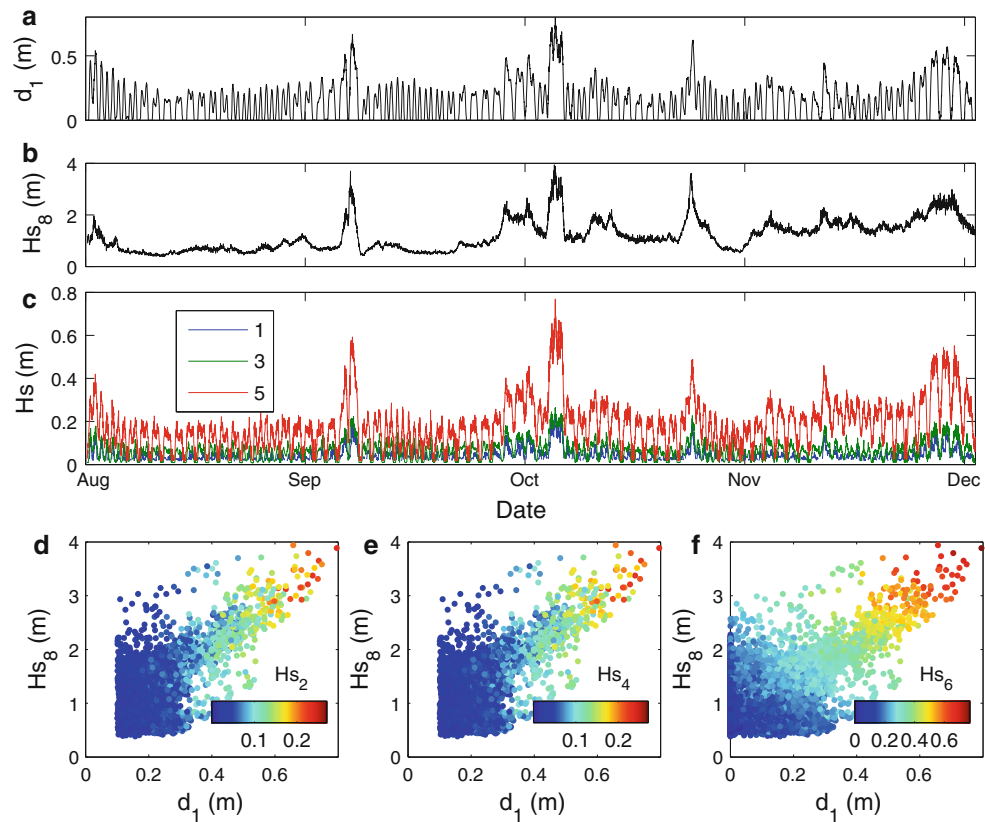
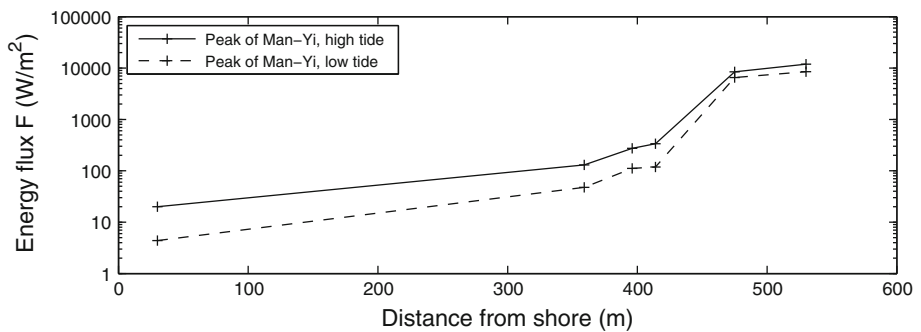


Fig. 6 Cross-shore SS energy flux profile across the reef for low tide (dash line) and high tide (solid line) at the peak of Man-Yi



observed for all sensors on the reef flat. Depth-limited breaking at the reef edge appears to influence significantly the transmission of SS wave energy on to the reef. The SS wave height is reduced by 90% between sensors 8 and 1 during high tide, 99% during low tide, and 97% averaged over all water depths.

Following Sheremet et al. (2002), we estimate that less than 5% of the incident SS wave energy flux is reflected at the fore reef (sensors 7 and 8) during deployment N . Of the incoming energy flux measured at 8 m depth on the fore reef, 83% of this energy flux remains at sensor 7, 2% at 5, and 0.1% at sensor 1 (Fig. 6). The region between sensors 7 and 6 corresponds to the location of a narrow breaker zone based on visual observations. These reductions in SS energy are consistent with previous studies (e.g., Young

1989; Kench 1998; Lugo-Fernandez et al. 1998a; Massel and Gourlay 2000; Brander et al. 2004).

The transformation of low frequency IG waves will be discussed in a separate paper, but estimates of the cross-shore components of IG and SS energy flux divergence are compared here to assess the possible importance of non-linear energy transfer ($\langle N \rangle$) in the SS energy balance (2). IG energy fluxes are estimated at the ADP sensors following Sheremet et al. (2002) and are integrated over the IG band (0.005–0.06 Hz). On the reef flat, inshore of the break point (from sensor 5 to sensor 1), the IG energy flux decays at a similar rate as the SS band, which we attribute to decay due to bottom friction. Offshore of sensor 5, the decrease in SS energy flux is an order of magnitude larger than the estimated changes in IG energy flux. While $\langle N \rangle$ is

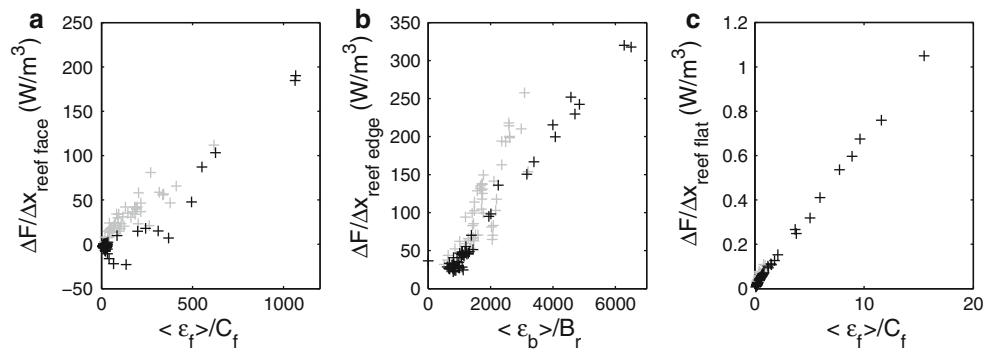


Fig. 7 Average rate of dissipation per unit area at **a** the fore reef (between sensors 8 and 7), **b** the reef crest (between sensors 7 and 5), and **c** the reef flat (between sensors 4/3 and 1 for deployment *G/N* plotted against the best matching parameterization of dissipation, which is $\langle \varepsilon_f \rangle / C_f$ from Eq. 4 for the fore reef and reef flat, and a wave

breaking parameterization $\langle \varepsilon_b \rangle / B_r$ from Eq. 3 for the reef crest. The breaking coefficient B_r (friction coefficient C_f) is estimated from the least square fit of $\langle \varepsilon_b \rangle / B_r(\langle \varepsilon_f \rangle / C_f)$ with the observed energy flux divergence. Deployment *N* is shown by the gray + and deployment *G* is shown with the black +

important in the IG energy balance, it is neglected with respect to the estimated dissipation in the SS energy balance (2).

We next compare the cross-shore energy flux divergence in the SS band with parameterizations of dissipation based on significant wave height (Eqs. 3 and 4). On the fore reef and the reef flat, the dependence of the SS energy flux divergence dF_{SS}/dx with significant wave height is approximately cubic (Fig. 7a, c), while near the reef crest the dependence is quadratic (Fig. 7b). For deployment *G*, the dependence of energy flux divergence on H_{rms}^3 on the reef flat (between sensors 4–1) is similar to that for deployment *N* on the reef flat (between sensors 3 and 1) (Fig. 7c). On the reef crest, between sensors 7 and 5, the observed quadratic dependence of the energy flux divergence with incident wave height (Fig. 7b) suggests dissipation due to breaking following the model of a saturated surf zone Eq. 3. We estimate the breaking parameter B_r by assuming that dissipation due to bottom friction between sensors 7 and 5 is negligible compared to the dissipation due to wave breaking. A least squares fit of Eq. 3 to the data in Fig. 7b gives a value of $B_r = 0.05$ (± 0.005 , 95% confidence interval estimated from independent data separated by 8 h) which is equivalent to the value used by Young (1989). This breaking parameterization does not account for steepness of the fore reef (Massel and Gourlay 2000), and the porous nature of the bottom near the reef edge and the value of B_r may implicitly incorporate these topographic and permeability effects. At Ipan where breaking is confined to a narrow section around the reef crest, a constant value of B_r independent of bottom characteristics is reasonable. B_r may however vary with wave conditions and this may explain the scatter of the points in Fig. 7b.

The reef flat and fore reef divergence are best fit with cubic wave height dependence (Fig. 7a, c). Estimation of

the friction coefficient by least squares fit of Eq. 4 to the data in Fig. 7a and c yields a value of $C_f = 0.06$ (± 0.02 , 95% confidence interval) on the reef flat and $C_f = 0.2$ (± 0.05) on the fore reef. The present estimates of C_f agree with values of f_w ($= 2 C_f$) determined for other reefs (e.g., $f_w = 0.1\text{--}0.7$, Ala Moana (Gerritsen 1981); $f_w = 0.1\text{--}0.7$, Ningaloo (Hearn 1999); $f_w = 0.07\text{--}0.22$, John Brewer reef (Nelson 1996); $C_f = 0.03\text{--}0.1$, Kaneohe (Hearn 1999)).

The spatial variability of the friction factor is related to the spatial variability of roughness length across the reef (Hearn 2011). The friction factor f_w has been related to bed hydraulic roughness or equivalent Nikuradse roughness height, r , (Swart 1974; Mirfenderesk and Young 2003). For a fully rough turbulent flow, Swart (1974) provides the following explicit formulation for f_w ,

$$f_w = \exp\left(5.213\left(\frac{r}{a}\right)^{0.194} - 5.977\right) \quad (5)$$

where a is the wave orbital diameter at the bed. Eq. 5 suggests that the friction factor is a function of the wave conditions through the orbital amplitude. Here, using the constant values estimated above, we compute the range of roughness that results from Eq. 5. On the fore reef, Eq. 5 yields a value of r between 1 and 4 m. On the reef flat, r ranges from 0.10 to 0.40 m. A roughness scale of order of meters is reasonable based on visual observations of the spur and groove structure on the reef face (Fig. 2). On the reef flat, roughness of tens of centimeters is reasonable for Ipan and comparable to roughness estimates on similar reefs (Nelson 1996; Nunes and Pawlak 2008).

Estimation of energy flux transformation

Reef flat SS wave heights scale with incident wave height and with water depth over the reef (Fig. 5). Because water depth on the reef also is correlated with incident wave

Table 2 Summary of parameters and input variables used for the different cases tested with the integration of the energy flux equation

	G	N	Indep. increase	Co-varying	Var. L	Var. Cf
Figure	9	9	10	11	Not shown	Not shown
B_r	0.075	0.075	0.075	0.075	0.075	0.075
γ_b	1.15	1.15	1.15	1.15	1.15	1.15
C_f slope	0.2	0.2	0.2	0.2	0.2	0–0.8
C_f flat	0.06	0.06	0.06	0.06	0.06	0–0.24
Bathy	Ipan	Ipan	Ipan	Ipan	Modified Ipan	Ipan
d_1	15-min tide	15-min tide	0–3 m	0–2 m	0–2 m	0–2 m
H_s	15-min H_s	15-min H_s	0–8 m	0–6 m	0–5 m	0–5 m
T_p	15-min T_p	15-min T_p	5–20 s	10 s	10 s	10 s

height due to wave setup, it is unclear to what extent the wave energy on the reef is depth-limited. To examine this issue as well as to consider reef flat wave heights for a greater range of conditions than observed, the friction, and wave breaking Eq. 3 energy loss parameterizations are used in a straight forward numerical integration of SS momentum and energy flux equations across the reef (from sensor 8 to sensor 1). The use of the 1D integration of the wave energy flux balance is intended as a tool to interpret the observations in the context of the simplest dynamics that governs the transformation. The equations are discretized using an explicit forward scheme. Inputs for the calculation are the bottom topography (Fig. 1), the 15-min mean tidal level d , incident significant wave height, H_s , and peak period, T_p , at sensor 8. The parameters and input variables used for each estimate are summarized in Table 2. The energy flux balance Eq. 2 is integrated with the bottom friction term $\langle \epsilon_f \rangle$ specified at every cross-shore grid point, the breaking term ϵ_b included in regions where the breaking criterion is met ($H_s \geq \gamma_b h$, $\gamma_b = 1.15$), and the non-linear term neglected everywhere yielding,

$$\frac{dF_{SS}}{dx} = \rho C_f \frac{1}{16\sqrt{\pi}} \left(\frac{2\pi\bar{f}}{\sinh kh} \right)^3 H_{rms}^3 + H(H_s - \gamma_b h) B_r \rho g \bar{f} H_b^2 \quad (6)$$

where H is the Heaviside step function and H_b is the breaking wave height equal to the local wave height if the breaking criterion is met. At each spatial increment ($s = 1$ m), the total depth is given by $h = d + \bar{\eta}$, where d is the tidally varying water level, assumed spatially constant across the reef, and $\bar{\eta}$ is the wave setup, which varies across the reef. Setup is computed using a 4th-order Runge–Kutta scheme to solve the mean momentum equation

$$\frac{d\bar{\eta}}{dx} = -\frac{1}{\rho g(\bar{\eta} + d)} \frac{dS_{xx}}{dx} \quad (7)$$

where S_{xx} is the cross-shore radiation stress (Longuet-Higgins and Stewart 1964). While wave dissipation is

included in the SS energy flux balance, dissipation due to the current boundary layer is neglected in the setup balance (Longuet-Higgins 2005). Vetter et al. (2010) demonstrate that the effects of dissipation appear to be small in the setup dynamics on the reef flat for Ipan. This is consistent with results from Symonds et al. (1995) for a wide shallow reef with narrow surfzone. At each time and space iteration, the cross-shore SS energy flux F_{SS} is used to compute the total SS energy E_{SS} , the significant wave height H_s , and the cross-shore radiation stress S_{xx} following

$$F_{SS} = c_g E_{SS} = \frac{1}{16} c_g \rho g H_s^2 \quad (8)$$

$$S_{xx} = E_{SS} \left(2\frac{c_g}{c} - \frac{1}{2} \right) \quad (9)$$

where c_g and c are the local group velocity and phase speed at the peak SS frequency. The choice of breaking criteria with respect to significant wave height $\gamma_b = 1.15$ is taken from the reported range of 0.4–1.8 (for a range of slope of 0.02–0.12) (Bowen et al. 1968; Tait 1972; Raubenheimer et al. 1996; Vetter et al. 2010), given the average reef face slope at Ipan of 0.07. This value of γ_b is consistent with the ratio of significant wave height to depth observed inshore of the break point at sensor 6 ($H_s/h = 1.4$) and with the values estimated by Vetter et al. (2010) for the same reef, with a single breakpoint model. We use $C_f = 0.2$ on the reef face and crest, and 0.06 on the reef flat.

The estimated cross-shore transformation of SS energy is in reasonable agreement with observed energy levels during energetic wave events (Fig. 8a). In particular, the sharp drop in energy through the surf zone (between sensors 7 and 5) is reproduced by the breaking parameterization, and the dissipation on the reef flat is accounted for by bottom friction. The correlation of observed and modeled H_{s1} ($\bar{\eta}_1$) is 0.89 (0.98) for deployment N and 0.97 (0.98) for deployment G . The simple dynamics of the 1D energy balance is in reasonable agreement with for the wave setup and the wave height transformation across the reef (Fig. 8b, c). During Man-Yi, the numerical runs

Fig. 8 **a** Comparison of total cross-shore SS energy during the peak event of N (*: 2 Oct. 2009, $H_s = 3.2$ m) and the peak of Man-Yi (Δ : 9 July 2007, $H_s = 4.3$ m). The solid lines are estimated energies computed from Eqs. 6–9 (see Table 2— N and G). Comparison of observed and estimated (Eqs. 6–9) **b** wave setup $\bar{\eta}_1$ and **c** significant wave height H_{s1} at the inner reef flat (sensor 1) (see parameters and inputs in Table 2) for deployments G (black crosses) and N (gray crosses)

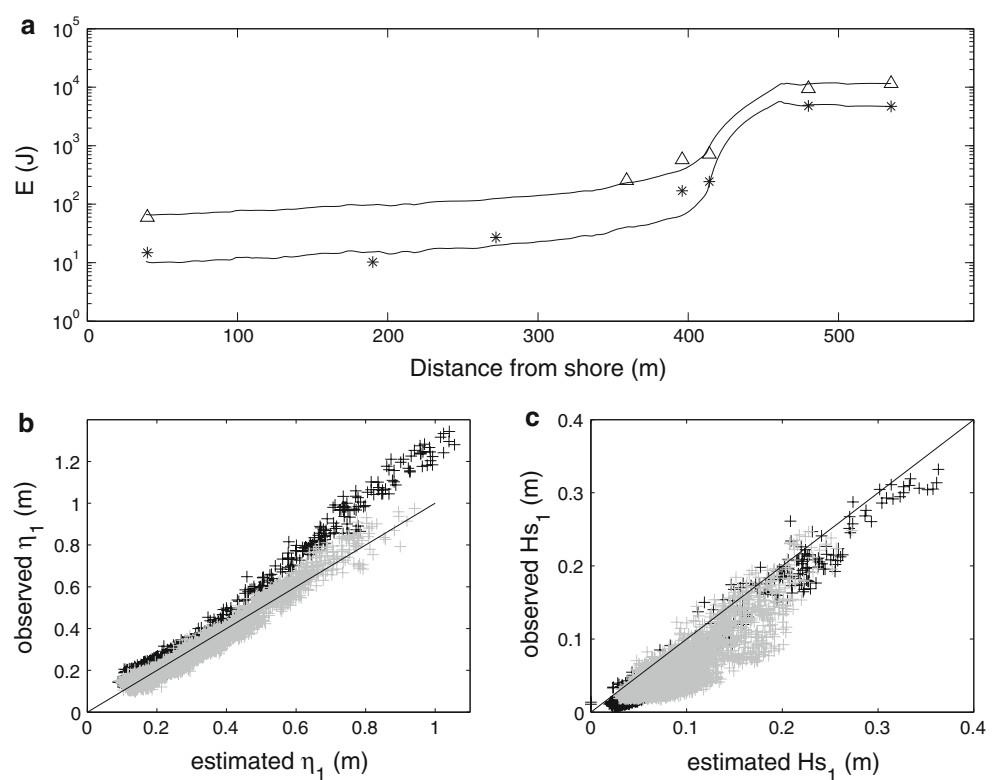
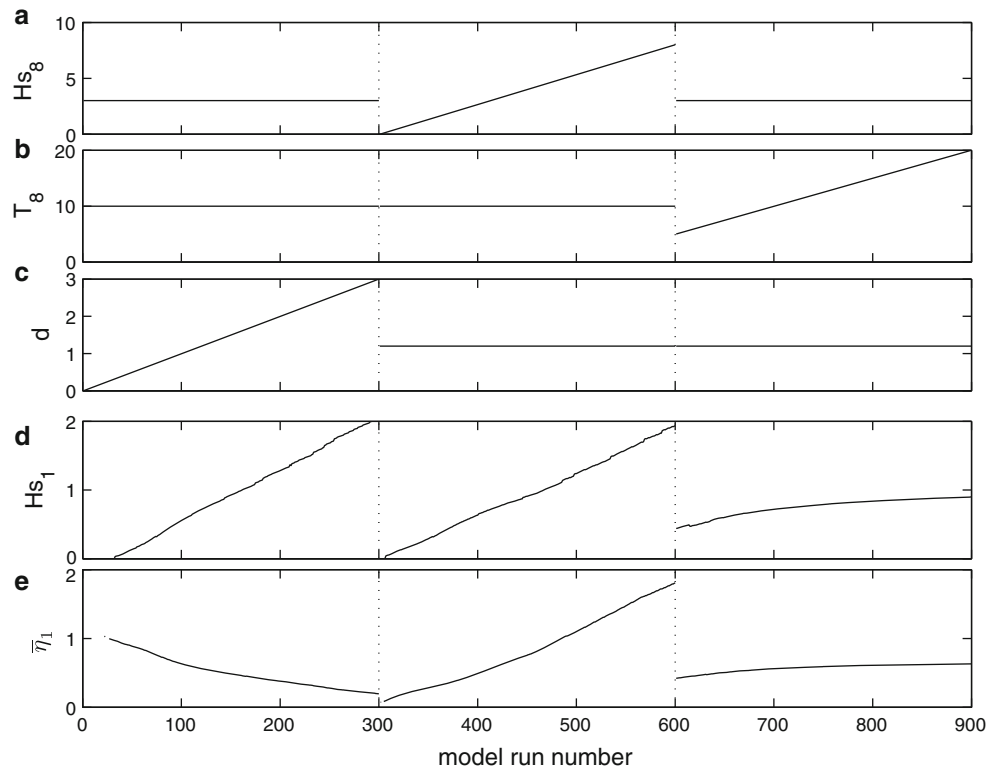


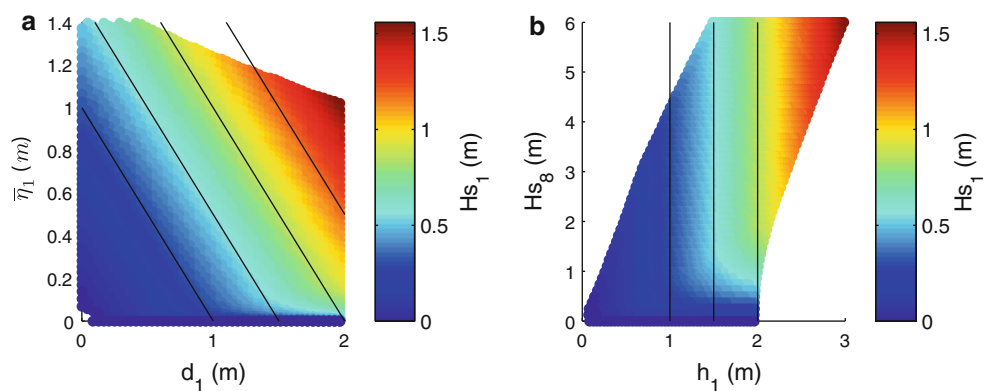
Fig. 9 Results of the numerical integration of Eqs. 6–9 showing the effect of an independent linear increase in three of the input variables. With all the other input variables remaining constant (values detailed in Table 2 “Indep. Increase”), **a** incident wave height, **b** incident wave period, and **c** water level are separately increased as shown and results in changes in **d** SS significant wave height H_{s1} and **e** setup $\bar{\eta}_1$ at the inner fore reef



underestimate the observed shoreline setup by about 30% (Fig. 8), possibly due to currents and non-wave-related sea level changes caused by winds during the storm.

We next investigate the effect of independently changing incident wave height (H_{s8}), and tidal level (d) on the shoreline significant wave height H_{s1} and setup $\bar{\eta}_1$ (Fig. 9)

Fig. 10 Effect of co-varying incident wave height and water level on SS significant wave height near the shore (H_{s1}) computed from Eqs. 6–9 using parameters and input variables summarized in Table 2 (co-varying). **a** H_{s1} as a function of tidal level d and setup $\bar{\eta}$ on the reef. **b** H_{s1} as a function of total depth on the reef h_1 and incident significant wave height H_{s8} . Black lines are line of equal water depth on the reef



using the integration of Eqs. 6–9. With all the other input variables remaining constant (see Table 2 “Indep. Increase” for values), the water level is linearly increased from 0 to 3 m for runs 1–300. The incident wave height is increased from 0 to 8 m for runs 301–600, and the incident wave period is increased from 5 to 20 s for runs 601–900. For a fixed incident wave height and period, wave height at the shoreline scales with water depth to the 1.38 power (Fig. 9, runs 1–300). The increase in H_{s1} occurs with a moderate decrease in setup associated with a reduction in the radiation stress gradient as more energy propagates on to the reef. For a fixed tidal height and wave period, the wave height on the reef flat increases with incident wave height (Fig. 9, middle panel). This increase is in part due to the increase in water depth on the reef from a nearly linear increase in wave setup (Fig. 9e). The increase in wave height on the reef with incident wave height and water depth has been reported previously (Young 1989; Hardy and Young 1996; Lugo-Fernandez et al. 1998c) for barrier reefs under moderate wave conditions. Changing the incident wave period within the range of observed values (5–15 s), while fixing tidal level and incident wave height, results in only small increases for both H_{s1} and $\bar{\eta}_1$ (Fig. 9, right panel).

We next focus on estimates of nearshore wave height for co-varying tidal level and incident wave height (Table 2 “co-varying”). The wave height near the shore is nearly constant for a given water depth on the reef regardless of whether the submergence is due to tides or wave setup (Fig. 10a). Over a minimum incident wave height threshold for a given water depth on the reef, the wave height at the shore is nearly independent of the incident wave height (Fig. 10b). For a reef configuration such as Ipan, where wave breaking is confined to a narrow zone around the reef crest, the threshold value is related to the shallowest depth observed at the reef crest. For waves smaller than γ_b times this depth, no breaking occurs and the wave height on the reef flat scales with incident wave height; for waves larger than γ_b times this depth, reef flat energy also increases with

incident wave height, but this is a result of setup increasing with wave height.

Wave heights just shore-side of the surf zone (roughly sensor 5) are determined by total water level; however, additional decay occurs across the reef due to wave friction (Fig. 5) so that narrower reef flats allow more energy to reach the shore. The wave height on the reef flat decreases nearly inversely with distance from the breaker zone. We find that reef width (defined as distance from the shore to the reef crest) does not affect setup significantly as previously observed in the laboratory by Seelig (1983).

Discussion

Wave data collected for a range of incident conditions are used to analyze the strong dissipation of SS wave energy across Ipan reef, Guam, which results in ~97% reduction in the incident wave height over ~500 m. Less than 5% of the incident energy flux is reflected at the fore reef. Of the remaining SS energy that propagates toward shore, >80% is dissipated due to wave breaking, 18% by bottom friction on the rough fore reef substrate ($C_f = 0.2$), and 2% by bottom friction on the wide reef flat ($C_f = 0.06$). These values of the friction factor are one and two orders of magnitude larger than the values observed on sandy beaches (Smyth and Hay 2002), but similar to value reported for other reefs (e.g., Gerritsen 1981; Nelson 1996; Hearn 1999).

As a result of the frictional dissipation, the decrease in wave height near the shore is inversely proportional to the width. Wave setup appears to be independent of reef width. This suggests that variation in coastal inundation along a shoreline with variable reef width and fixed incident wave height may be due to variable swash (e.g., inundation reports for the south shore of Guam during Typhoon Russ by Jaffe and Richmond 1993).

Previous attempts to model wave dissipation across a proto-typical Guam fringing reef based on parameterizations

developed using laboratory data (Massel and Gourlay 2000) produce qualitatively similar results to those presented here, with the majority of dissipation occurring in the surf zone. Water depth on the reef strongly controls the amount of SS energy that reaches the shore, consistent with wave dissipation being dominated by a depth-limited breaking process. Our observations show that the increase in reef flat wave heights with increasing incident wave height is primarily due to the linear increase in reef flat water depth due to wave setup. The water level on the reef, whether due to tides or setup, determines the reef flat wave height. This holds when the breaker zone is a limited region near the reef edge, as is the case for our observations. We speculate that the breaker zone may extend across the reef flat for extreme typhoon conditions, in which case nearshore wave heights may well exceed levels predicted here (i.e., larger than Fig. 10 would indicate).

This paper emphasizes the importance of water level on the reef flat for coastal inundation. The potential effect of sea level rise on wave transformation over Ipan reef (assuming no change in topography) would be twofold: higher reef flat water levels would allow more sea and swell energy to reach the shore, but also would result in a moderate decrease in wave setup (Fig. 9, left panel). The projected impact on coastal wave energy must take into account both of these effects. For example, an increase in sea level of 0.5 m over a range of incident wave height of 1–5 m yields an increase in SS wave height near the shore of 25 cm despite a 6 cm decrease in wave setup.

Acknowledgments We thank J. Miller and the staff of the University of Guam Marine Laboratory, and C. Kontoes, O. Vetter, T. Hilmer, C. Quisenberry, J. Aucan, K. Millikan, Y. Firing, G. Rocheleau, A. Fetheroff, and P. Lethaby from SOEST, University of Hawaii for their outstanding contributions to the field operations in Guam. The wave buoy data were provided by the Coastal Data Information Program (CDIP) at the University of California, San Diego (UCSD). PILOT project support provided by J. Thomas (UCSD) and R. Jensen and A. Garcia (US-ACE) is greatly appreciated. The two reviewers and the topic editor's comments are appreciated. PILOT was funded by the U. S. Army Corps of Engineers via a subcontract PO 10230553 from the University of California, San Diego. ACP was partially funded by a grant/cooperative agreement from the National Oceanic and Atmospheric Administration, Project R/EP-31, which is sponsored by the University of Hawaii Sea Grant College Program, SOEST, under Institutional Grant No. NA05OAR4171048 from NOAA Office of Sea Grant, Department of Commerce. The views expressed herein are those of the authors and do not necessarily reflect the views of NOAA or any of its subagencies.

References

- Baldock TE, Holmes P, Bunker S, van Weert P (1998) Cross-shore hydrodynamics within an unsaturated surf zone. *Coast Eng* 34:173–196
- Battjes JA, Janssen JPJM (1978) Energy loss and set-up due to breaking of random waves. Proceedings of the 16th international conference on coastal engineering conference, American Society of Civil Engineers, pp 569–587
- Bowen AJ, Inman DL, Simmons VP (1968) Wave set-down and wave set-up. *J Geophys Res* 73(8):2569–2577
- Brander RW, Kench PS, Hart D (2004) Spatial and temporal variations in wave characteristics across a reef platform, Warraber Island, Torres Strait, Australia. *Mar Geol* 207(1–4): 169–184
- Burbick DR (2005) Guam coastal atlas. Report 114, University of Guam Marine Laboratory, Mangilao
- Gerritsen F (1981) Wave attenuation and wave set-up on a coastal reef. Technical report. Look Lab, Univ. Hawaii, Honolulu
- Gourlay MR (1996a) Wave set-up on coral reefs. 1. Set-up and wave-generated flow on an idealized two dimensional horizontal reef. *Coast Eng* 27(3–4):161–193
- Gourlay MR (1996b) Wave set-up on coral reefs. 2. Set-up on reefs with various profiles. *Coast Eng* 28(1–4):17–55
- Gourlay MR, Collette G (2005) Wave-generated flow on coral reefs—an analysis for two-dimensional horizontal reef-tops with steep faces. *Coastal Eng* 52(4):353–387
- Hardy TA, Young IR (1996) Field study of wave attenuation on an offshore coral reef. *J Geophys Res* 101(C6):14,311–14,326
- Hearn CJ (1999) Wave-breaking hydrodynamics within coral reef systems and the effect of changing relative sea level. *J Geophys Res* 104(C12):30007–30019
- Hearn CJ (2011) Hydrodynamics of coral reef systems. In: Hopley D (ed) Encyclopedia of Modern Corals. Springer
- Jaffe BE, Richmond BM (1993) Overwash variability on the shoreline of Guam during Typhoon Russ. *Proc 7th Int Coral Reef Symp* 1:257–264
- Kench PS (1998) Physical processes in an Indian Ocean atoll. *J Coast Res* 17(2):155–168
- Kench PS, Brander RW (2006) Wave processes on coral reef flats: Implications for reef geomorphology using Australian case studies. *J Coast Res* 22(1):209–223
- Lobban CS, Scheffer M (1994) Tropical pacific island environments, 2nd edn. University of Guam Press, Guam
- Longuet-Higgins MS (2005) On wave set-up in shoaling water with rough sea bed. *J Fluid Mech* 527:217–234
- Longuet-Higgins MS, Stewart RW (1964) Radiation stress in water waves, a physical discussion with applications. *Deep-Sea Res* 11:529–563
- Lowe RJ, Falter JL, Bandet MD, Pawlak G, Atkinson MJ, Monismith SG, Koseff JR (2005) Spectral wave dissipation over a barrier reef. *J Geophys Res* 110(C04001). doi:10.1029/2004JC002711
- Lugo-Fernandez A, Roberts HH, Wiseman WJ (1998a) Tide effects on wave attenuation and wave set-up on a caribbean coral reef. *Estuar Coast Shelf Sci* 47(4):385–393
- Lugo-Fernandez A, Roberts HH, Suhayda JN (1998b) Wave transformations across a Caribbean fringing-barrier coral reef. *Cont Shelf Res* 18(10):1099–1124
- Lugo-Fernandez A, Roberts HH, Wiseman WJ, Carter BL (1998c) Water level and currents of tidal and infragravity periods at Tague Reef, St. Croix (USVI). *Coral Reefs* 17(4):343–349
- Massel SR (1996) Ocean surface waves: their physics and prediction. Advanced series on ocean engineering! V. 11. World Scientific
- Massel SR, Gourlay MR (2000) On the modelling of wave breaking and set-up on coral reefs. *Coast Eng* 39:1–27
- Mirfendereski H, Young IR (2003) Direct measurements of the bottom friction factor beneath surface gravity waves. *Appl Ocean Res* 25:269–287
- Monismith S (2007) Hydrodynamics of coral reefs. *Annu Rev Fluid Mech* 39:37–55

- Munk WH, Sargent MC (1948) Adjustment of Bikini atoll to ocean waves. *Trans Am Geophys Union* 29:855–860
- Nelson RC (1996) Hydraulic roughness of coral reef platforms. *Appl Ocean Res* 18:265–274
- Nunes V, Pawlak G (2008) Observations of bed roughness of a coral reef. *J Coast Res* 24(2B):39–50
- Péquignet ACN, Becker JM, Merrifield MA, Aucan J (2009) Forcing of resonant modes on a fringing reef during tropical storm Man-Yi. *Geophys Res Lett* 36. doi:[10.1029/2008GL036259](https://doi.org/10.1029/2008GL036259)
- Raubenheimer B, Guza RT (1996) Observations and predictions of run-up. *J Geophys Res* 101(C11):25575–25587
- Raubenheimer B, Guza RT, Elgar S (1996) Wave transformation across the inner surf zone. *J Geophys Res* 101(C10):25,589–25,597
- Ruggiero P, Holman R, Beach R (2004) Wave run-up on a high-energy dissipative beach. *J Geophys Res* 109. doi:[10.1029/2003JC002160](https://doi.org/10.1029/2003JC002160)
- Seelig WN (1983) Laboratory study of reef-lagoon system hydraulics. *J Waterw Port Coastal Ocean Eng ASCE* 109:380–391
- Sheremet A, Guza RT, Elgar S, Herbers THC (2002) Observations of nearshore infragravity waves: Seaward and shoreward propagating components. *J Geophys Res* 107. doi:[10.1029/2001JC000970](https://doi.org/10.1029/2001JC000970)
- Smyth C, Hay AE (2002) Wave friction factors in the nearshore sands. *J Phys Oceanogr* 32(12):3490–3498
- Swart D (1974) Offshore sediment transport and equilibrium beach profiles. Technical report 131, Delft Hydraulic Laboratory, Netherlands
- Symonds G, Black KP, Young IR (1995) Wave-driven flow over shallow reefs. *J Geophys Res* 100(C2):2639–2648
- Tait RJ (1972) Wave setup on coral reefs. *J Geophys Res* 77(C10):2207–2211
- Thornton EB, Guza RT (1983) Transformation of wave height distribution. *J Geophys Res* 88(C10):5925–5938
- Vetter OJ, Becker JM, Merrifield MA, Péquignet AC, Aucan, J, Boc SJ, Pollock CE (2010) Wave setup over a pacific island fringing reef. *J Geophys Res* (in press)
- Young IR (1989) Wave transformations on coral reefs. *J Geophys Res* 94(C7):9779–9789